Electrodeposition of CdTe thin films onto n-Si(1 0 0): nucleation and growth mechanisms

H. Gómez[a,*], R. Henríquez[a], R. Schrebler[a], R. Córdova[a], D. Ramírez[a], G. Riveros[a,b], E.A. Dalchiele[c]

[a] *Facultad de Ciencias, Instituto de Química, Pontificia Universidad Católica de Valparaíso, Casilla 4059, Valparaíso, Chile*
[b] *Departamento de Química, Facultad de Ciencias, Universidad de Chile, Casilla 653, Santiago de Chile, Chile*
[c] *Facultad de Ingeniería, Instituto de Física, Herrera y Reissig 565, C.C. 30, 11000 Montevideo, Uruguay*

Abstract

The mechanisms related to the initial stages of the nucleation and growth of cadmium telluride (CdTe) thin films on the rough face side of a (1 0 0) monocrystalline n-type silicon have been studied as a function of different potential steps that varied from an initial value of −0.200 V to values comprised between −0.515 and −0.600 V versus saturated calomel electrode (SCE). The analysis of the corresponding potentiostatic *j*/t transients suggests that the main phenomena involved at short times is the formation of a Te–Cd bi-layer (BL). For potentials below −0.540 V, the formation of this bi-layer can be considered independent of potential. At greater times, the mechanisms is controlled by two process: (i) progressive nucleation three dimensional charge transfer controlled growth $(PN\text{-}3D)_{ct}$ and (ii) progressive nucleation three dimensional diffusion controlled growth $(PN\text{-}3D)_{diff}$, both giving account for the formation of conical and hemispherical nuclei, respectively. Ex situ AFM images of the surface seem to support these assumptions.

Keywords: Electrodeposition; Cadmium telluride; Monocrystalline silicone substrate; Rough face; Nucleation and growth mechanism

1. Introduction

Chalcogenide cadmium telluride (CdTe), is recognized as a highly versatile II–VI narrow bandgap binary compound semiconductor (E_g = 1.45 eV) [1], from which one can expect a high solar energy conversion efficiency. This compound is the only binary II–VI material which can be in both n- and p-conductivity types [2]. Furthermore, the direct optical transition results in a large absorption coefficient that makes the use of thin film solar cells possible. Its applications range from solar cells to gamma-ray and infrared detectors [3]. In addition, its close lattice match and chemical compatibility with HgCdTe make CdTe an ideal substrate for growth of this variable band-gap infrared detector material [4,5]. Lately, these materials are generating great interest because their properties are well suited for the fabrication of nuclear radiation detectors operating at room temperature [6]. On the other hand, silicon is appealing as a substrate material because of its transparency to infrared radiation out to wavelengths beyond 14 μm and because large-area wafers of the highest structural perfection are readily available commercially at a minimal cost. In addition, Si integrated circuit processing technologies are well developed and can be combined readily with selected area $Hg_xCd_{1-x}Te$/CdTe/Si heteroepitaxy to form the monolithic infrared detecting systems [3,4,7].

The growth of CdTe on silicon is driven mainly by infrared applications. CdTe/Si is now being used for the fabrication of megapixel HgCdTe hybrid infrared focal plane arrays (IRFPAs) [4], which will find very large applications in military, space and medical imaging areas for infrared imaging and low-background detection.

* Corresponding author. Tel.: +56 32 273173; fax: +56 32 273422.
E-mail address: hgomez@ucv.cl (H. Gómez).

Various growth techniques, such as molecular-beam epitaxy (MBE) [7–9], metalorganic chemical vapor deposition (MOCVD) [10,11], UHV sublimation [12], metalorganic vapor phase epitaxy (MOVPE) [13] and hot wall epitaxy [14,15] have been used to grow CdTe films onto silicon substrates. Notwithstanding, low-temperature, in situ fabrication of crystalline thin films, is essential in order to improve their quality, lower production costs, and make the whole process environmentally friendly. Electrodeposition is a well adapted alternative technique that has been successfully used for thin film preparation. However, electrodeposition onto Si is very difficult and hard, the quality of the Si substrate surface greatly influences the quality of the subsequent layers. For instance, the native oxide formation leads to passivity problems. Meticulous care has to be taken in preparing the Si surface prior to electrodeposition in order to avoid adventitious surface oxide formations as well as to eliminate the spontaneous deposition of tellurium on the Si surface. The difficulty of obtaining CdTe thin films of good quality by electrodeposition onto Si, appears to be an important challenge. Sugimoto and Peter [16,17], and Berlouis group [18,19], investigated the CdTe electrodeposition onto flat silicon single crystals. More recently, Takahashi et al. [20], presented results on epitaxial grown of CdTe films by electrodeposition onto Si(1 1 1), assisted by pulsed-light (from a xenon lamp).

Formation of a homogeneous film can be reached with an ideally energetically uniform surface, condition that in practice is unreachable. An alternative approach can be explored, consisting in using a substrate with a very high density of surface non-uniformities [21]. This approach will lead to a macroscopic equalization of injection conditions for electrons all along the surface, resulting in a uniform deposit growing [21]. The rear side of one side polished silicon wafer (the rough face side of the silicon wafer) contains this type of in-homogeneities. Results on the electrodeposition of CdTe thin films onto the rough face side of a n-type silicon (1 0 0) wafer, have been recently reported by our group [22]. The electrodeposits formed on this substrate shown a good adherence as well as a (Cd/Te) atomic ratio very close to one. However, the formation of a continuous and a good quality thin film requires a detailed understanding of the nucleation and growth mechanisms. To our knowledge, only the work of Peter et al. about nucleation and growth of the electrodeposition of CdTe onto n-Si with different surface orientations ((1 0 0), (1 1 1) and (110)), can be found in the literature [16,17]. In current work, results of the study on nucleation and growth mechanisms of the electrodeposition of CdTe onto the rough face of a n-Si(1 0 0) are presented.

2. Experimental

Nucleation and growth mechanism studies were performed on the rough face side of a (1 0 0) monocrystalline n-type silicon (1.0–5.5 Ω cm. P-doped, Int. Wafer Service, CA, USA), which was chosen because it gives a nonblocking electrode for cathodic reactions in dark conditions. The wafer was cut in small 1 cm × 1 cm squares that were first degreased in boiling isopropanol, and then rinsed with a 0.5:1:4 $HCl:H_2O_2:H_2O$ mixture heated up to 80 °C, in order to remove any trace of heavy metals. Afterwards, the oxide film was removed by etching with a 2 M HF acid (pH 4.5) solution and thoroughly rinsed with ultra pure water. The ohmic contact was made through the application of a Ga–In eutectic in the polished face of the samples that were mounted in a copper support. The edges of the silicon squares and the copper were isolated with an adhesive Teflon tape, leaving a defined exposed area of 0.30 cm^2 facing the solution. Before running the electrochemical experiments the electrode surface was again etched for 15 min with the 2 M HF solution (after this procedure an atomically smooth and predominantly hydrogen terminated surface, H-terminated n-Si(1 0 0), would be obtained [23,24]). The electrolytic solutions were prepared from analytical grade reagents with the following compositions: 1 mM TeO_2 + 0.5 M $CdSO_4$ + 0.5 M H_2SO_4 + 0.5 M NH_4F (pH = 0.29 at 20 °C as room temperature).

Electrochemical experiments were conducted in darkness at 85 °C to obtain a good crystalline structure of the deposits [18,19,25]. Prior to the experiment the electrolytic solutions were de-aerated by purging with 5N nitrogen. To keep the cell atmosphere free of oxygen during the measurement nitrogen was passed over the electrolyte. A platinum wire served as the counter-electrode, and a saturated calomel electrode (SCE) was used as the reference (all the potentials in this work will be referred to this SCE). To minimize the formation of a Te layer, at the point of immersing the working electrode into solution, the potential was set at −0.200 V employing a platinum probe.

The electrochemical measurements were done using model IM6e BAS–ZAHNER impedance measurement unity, and electrodepositions were carried out using model 263A EG&G Princeton Applied Research potentiostat. The AFM images were obtained with a Digital Instrument (NANOSCOPE IIIA Series) using the contact mode at a scan rate of 0.02 $\mu m\, s^{-1}$.

The data analysis was performed using a commercial software package (ORIGIN™ from MicroCal Software Inc.). The non-linear least square procedure fitting for the simulation of the *j*/t transients was based on the Levenberg–Marquardt algorithm.

3. Results and discussion

3.1. Voltammetric study

In order to understand the CdTe nucleation and growth mechanism on silicon, is important to know the electrochemical response of the rear side of the one sided polished n-Si(1 0 0) wafer, which is the substrate studied in present work. In the following the rough face refers to the rear side of one side polished wafer whose cyclic voltammetric response in

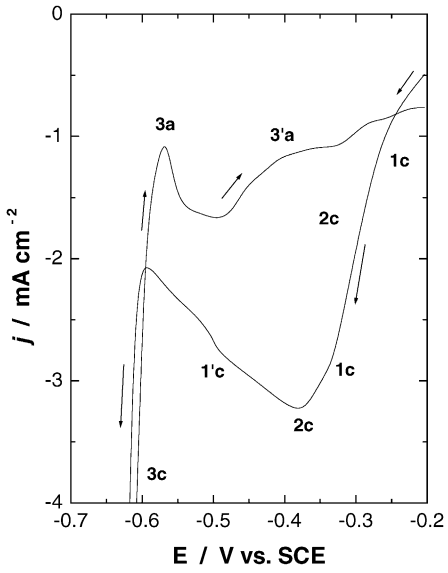

Fig. 1. Cyclic voltammogram of a n-Si(1 0 0) electrode (rough side), in 0.5 M $CdSO_4$ + 1 mM TeO_2 + 0.5 M H_2SO_4 + 0.5 M NH_4F. Scan rate: 10 mV s^{-1}. Temperature: 85 °C. The arrows denote the direction of the potential scan.

a electrodeposition bath containing Cd and Te precursors in the presence of 0.5 M NH_4F at a temperature of 85 °C is depicted in Fig. 1. The small cathodic shoulder (1c) at −0.325 V can be associated to $HTeO_2^+$ reduction to tellurium through a four electron process:

$$HTeO_2^+ + 3H^+ + 4e^- \Leftrightarrow Te^0 + 2H_2O \quad (1)$$

with an equilibrium potential, $U_{eq}{}^0$ = +0.278 V versus SCE. In agreement with Kröger theory [26], the broad current peak at −0.380 V (2c) is related to the electrodeposition of CdTe through a two-electron process,

$$Cd^{2+} + Te^0 + 2e^- \Leftrightarrow CdTe \quad (2)$$

Extending the scan towards more negative potential a small shoulder (1′c) is observed at ca. −0.500 V which is probably related to the reduction of Te to H_2Te [27]. This process is followed by a current decay until a potential of −0.600 V is reached. Beyond −0.600 V, the cathodic current (3c) that increases almost linearly with potential may be associated to the deposition of metallic Cd which is present in a substantial concentration in the bath. The small peak (3a) observed during the anodic scan indicates that only a fraction of the electrodeposited Cd is stripped at this potential interval and most of cadmium stripping is associated to the wide shoulder denominated as (3′c). This is probably due to the fact that as the metal is in direct contact with the CdTe semiconductor film, a higher overpotential is needed to produce the re-oxidation. Further, the anodic stripping of CdTe is not observed in this potential range, probably due to the presence of a Schottky barrier at the n-Si(1 0 0) surface. The fact that the current remains cathodic indicates a lower electrodeposition over-voltage on an already coated surface.

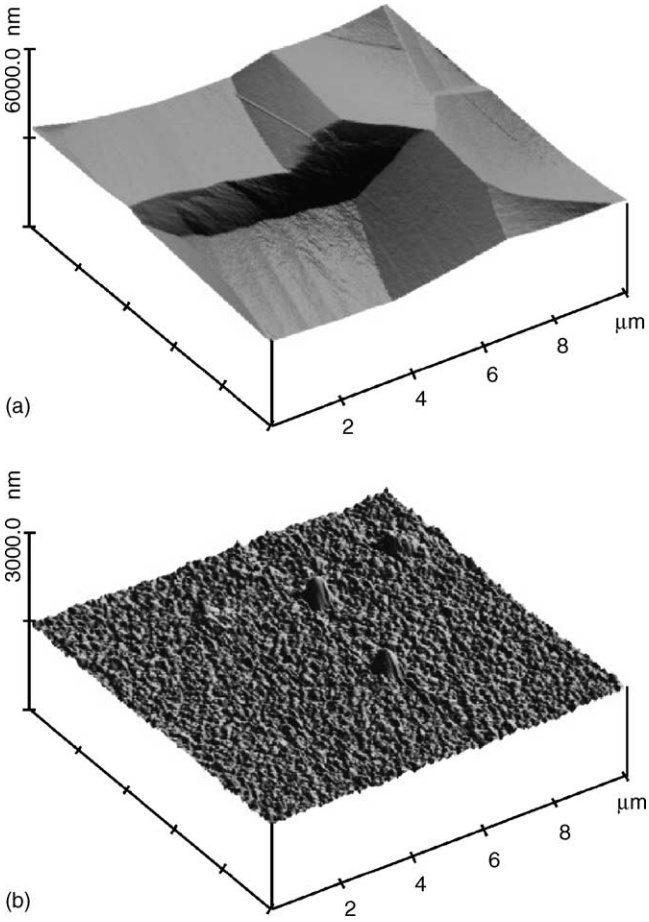

Fig. 2. AFM images of (a) rough side of n-Si(1 0 0) and (b) CdTe film deposited at E_d = −0.545 V vs. SCE on silicon substrate, q_d = −0.319 C cm^{-2}.

It is worth noting that in the potential interval between −0.380 and −0.500 V, the deposition of CdTe may be accompanied by the formation of a Te excess. On the other hand, in the potential interval where the metallic cadmium electrodeposition takes place (−0.500 to −0.580 V), stoichiometric CdTe deposition should be expected. In fact, energy dispersive X-ray spectroscopy analysis showed that in this potential range CdTe thin films with Cd/Te atomic ratios close to one are obtained [28].

3.2. Morphological study

Morphological characterization of both, silicon rough surface and electrodeposited CdTe thin film, were done by AFM analysis. Fig. 2a shows the as received surface structure of the rough face of a n-Si(1 0 0) where the presence of inverted pyramids can be observed. These pyramidal texturing can be attributed to the combination of anisotropic etching of the silicon surface, and to hydrogen bubbles evolved during the etching reaction [29]. According to Table 1, there is not a significant difference between the roughness coefficient in both sides of the Si wafer but, due to the presence of the pyramids, the RMS values are remarkable different. Accordingly, the

Table 1
Roughness coefficient obtained by roughness analysis in AFM images for both n-Si(1 0 0) wafer sides and CdTe as electrodeposit on rough silicon

Material	Geometric area (μm^2)	Surface area (μm^2)	Roughness coefficient	RMS (nm)
Flat – Si	100.00	100.00	1.0000	1.698
Rough – Si	100.00	102.66	1.0266	191.000
Rough – Si/CdTe	100.00	112.36	1.1236	32.490

real surface area in rough silicon substrate is not extremely different to the calculated geometric area. Fig. 2b shows an AFM image of an as-grown electrodeposited CdTe film (1 μm thickness, $E_{dep} = -0.575$ V), onto this rough silicon surface. The film presents a smooth aspect, with a cauliflower microstructure. Moreover, inside of this surface some conical nucleus can be seen.

3.3. Nucleation and growth mechanism analysis

The comparison between the *j*/t transient responses for the formation of a CdTe film shows remarkable differences in the nucleation and growth mechanism for both sides of a n-Si(1 0 0) wafer(Fig. 3a). Whereas on the flat side the current undergoes an exponential decay with time, the rough side exhibits a well developed process associated to the nucleation of a phase at the electrode surface. The increase in the nucleation kinetics of the rough face can be related to the presence of terraces that supply a significative number of edges that energetically favors the adsorption and further reduction of the redox species that are present at the interface. In fact, studies conducted for other authors [16–19] demonstrate that the growth of a thick CdTe layer on a flat n-Si(1 0 0) surface is not possible due to the poor adherence of the film. Instead,

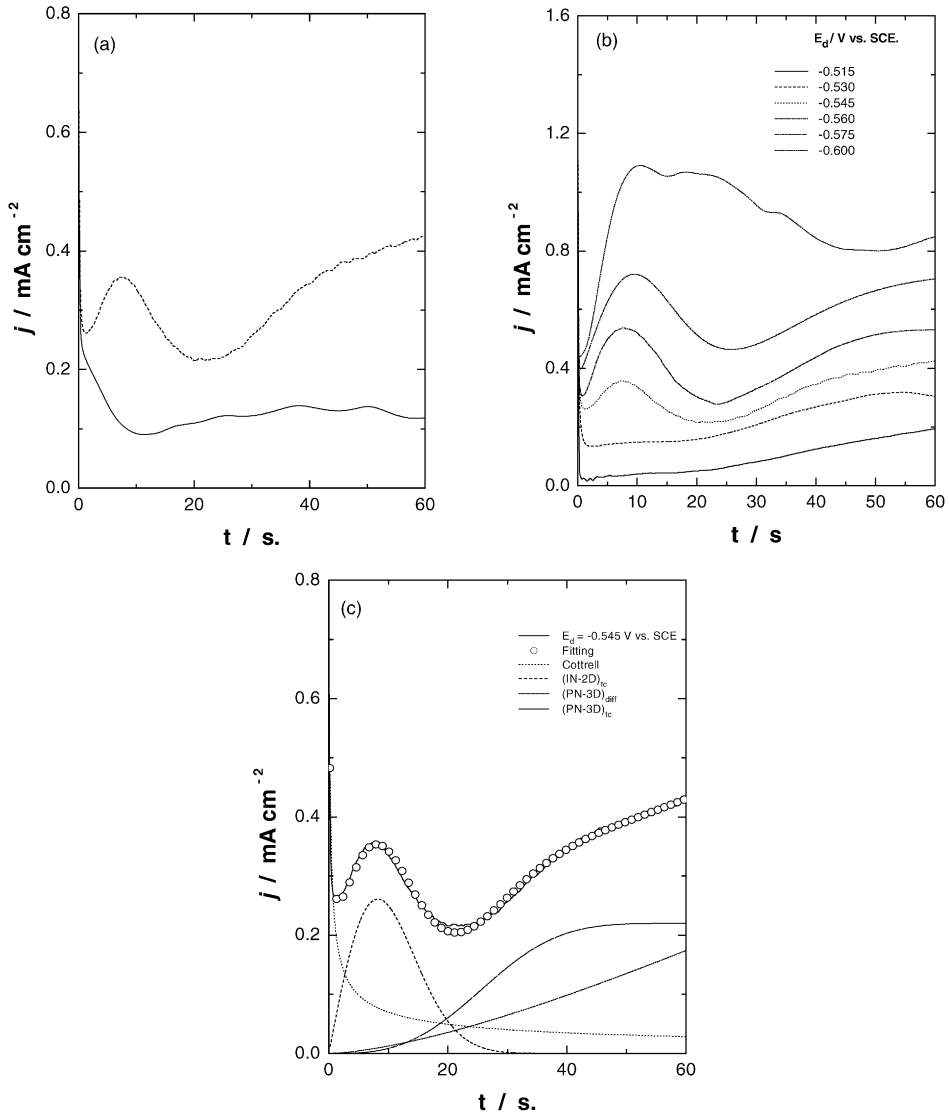

Fig. 3. (a) Comparison between two *j*/t transient obtained at $E_d = -0.545$ V vs. SCE on rough (- - - -) and flat (—) n-Si(1 0 0). (b) Experimental *j*/t transients recorded on a n-Si(1 0 0) rough face using 0.5 M $CdSO_4$ + 1 mM TeO_2 + 0.5 M H_2SO_4 + 0.5 M NH_4F as deposition bath, (c) *j*/t transient fitting for $E_d = -0.545$ V vs. SCE. All the simulation values are shown in Table 2.

Table 2
Fitting parameter values for CdTe *j*/t transients and nucleation and growth mechanisms proposed

E_d/V vs. SCE	N.G.M.: Cottrell + $(IN\text{-}2D)_{tc}$ + $(PN\text{-}3dD)_{diff}$ + $(PN\text{-}3D)_{tc}$; equation: $i[A] = \frac{P_1}{t^{1/2}} + P_2 t \times \exp^{-P_3 t^2} + \frac{P_4}{t^{1/2}}[1 - \exp^{-P_5 t^2}] + P_6[1 - \exp^{-P_7 t^3}]$						
	$P_1 = \frac{anFD^{1/2}C^{\infty}}{\pi^{1/2}}$ (A s$^{1/2}$)	$P_2 = \frac{2\pi nFMhN^{\circ}k^2}{\rho}$ (A s^{-1})	$P_3 = \frac{\pi M^2 N^{\circ} k^2}{\rho^2}$ (s^{-2})	$P_4 = \frac{anFD^{1/2}C^{\infty}}{\pi^{1/2}}$ (A s$^{1/2}$)	$P_5 = A'\pi KD$ (s^{-2})	$P_6 = anFk'_3$ (A)	$P_7 = \frac{\pi M^2 k_3^2 A_3 N^{\circ}}{3\rho^2}$ (s^{-3})
−0.515	1.960×10^{-5}	4.09×10^{-6}	0.00582	9.6670×10^{-3}	3.0×10^{-5}	5.752×10^{-5}	2.0×10^{-5}
−0.530	1.550×10^{-4}	1.342×10^{-5}	0.00407	10.557×10^{-3}	1.0×10^{-5}	2.450×10^{-4}	3.0×10^{-5}
−0.545	2.210×10^{-4}	5.231×10^{-5}	0.00739	10.053×10^{-3}	4.0×10^{-5}	2.204×10^{-4}	4.0×10^{-5}
−0.560	1.474×10^{-4}	7.550×10^{-5}	0.00720	9.981×10^{-3}	1.0×10^{-5}	3.411×10^{-4}	2.0×10^{-5}
−0.575	1.825×10^{-4}	6.919×10^{-5}	0.00572	6.405×10^{-3}	2.0×10^{-5}	3.711×10^{-4}	2.0×10^{-5}

E_d: Potential step value; N°: number of active sites under the experimental conditions (cm^{-2}); *A:* bi-dimensional nucleation rate constant (cm^{-2} s^{-1}); *k*: bi-dimensional incorporation constant rate (mol cm^{-2} s^{-1}); *h*: height of bi-dimensional nuclei (cm); *n*: electron number; *F*: Faraday constant (A s mol^{-1}); *a*: electrode area (cm^2); *M*: molar mass (g mol^{-1}); ρ: density (g cm^{-3}); C^{∞}: concentrations in bulk solution (mol cm^{-3}); *D*: diffusion coefficient (cm^2 s^{-1}); k'_3: horizontal incorporation constant rate (mol cm^{-2} s^{-1}); k_3: perpendicular incorporation constant rate (mol cm^{-2} s^{-1}); A_3: three dimensional constant rate (cm^2 s^{-1}). With $K = 4/3(8\pi C^{\infty} M/\rho)^{1/2}$, $A' = AN^{o}$.

our results show that the imperfections that are present on the rough side allow to successfully grow an adherent and thick CdTe film.

To study the nucleation and growth mechanism of CdTe on the unpolished side of the (1 0 0) silicon wafer a set of *E*/*t* perturbation programs (including different potential steps), were employed. Fig. 3b shows the respective *j*/t transients recorded between an initial potential of −0.200 V and a final value varying from −0.515 to −0.600 V. After the initial double layer charging, they firstly exhibit an induction time of about 1–2.5 s followed by a current increase associated to the solid phase formation. The further evolution depends on the final applied potential. An almost linear current increase is observed for the more positive values but, from −0.530 V two new contributions appear: one in the interval between 5 to 20 s and the other after 20 s.

At −0.600 V there are other current contributions that are probably related to the deposition of a cadmium excess. The fitting of the curves was made employing the general equation presented in Table 2 for the transients recorded between −0.515 and −0.560 V (i.e. −0.545 V, Fig. 3c). This general equation has been constructed considering the addition of the currents contributions and the theoretical nucleation and growth mechanisms (NGM) that have been reported in the literature [30,31]. The parameters P1–P7 used in the *j*/t transient fitting are described in Table 2 and the meaning of each term is indicated in the same table. The following deconvoluted contributions were obtained: at very short interval times appears first the double layer charging, followed by a Cottrell type current decay related to the multielectronic electroreduction of $HeTO_2^+$ ions to tellurium. The corresponding calculated diffusion coefficient considering the real area of the rough silicon electrode gives a value of $D_{Te} = 1.07 \times 10^{-5}$ cm^2 s^{-1} (close to that previously reported by Mori and Rajeshwar [29] (1.14×10^{-5} cm^2 s^{-1}). The last contribution corresponds to the starting of the nucleation and growth processes which is initially related to the 2D Te nuclei formation. It is worth noting that the t_{max} values of this 2D contribution do not follow the typical behavior expected when E_d is moved towards more negative values. In fact, at $E_d = -0.515$ V t_{max} is located at 9.2 s but at −0.530 V, instead of finding a lower t_{max} this is higher (10.8 s) than expected. A possible explanation of this behavior can be associated to the fact that at more negative potentials starts the simultaneous deposition of tellurium and cadmium a process which should present a coalescence time different than that of tellurium alone. As E_d is made more negative ($E_d \geq -0.560$ V) the 2D process is now associated to a Cd–Te bi-layer (BL), with its own time constant, and the t_{max} decreases as expected. At $E_d = -0.575$ V, t_{max} again increases a fact that can be explained assuming that at this potential value the Cd and Te ad-atoms that are forming at the electrode surface are distributed between the three

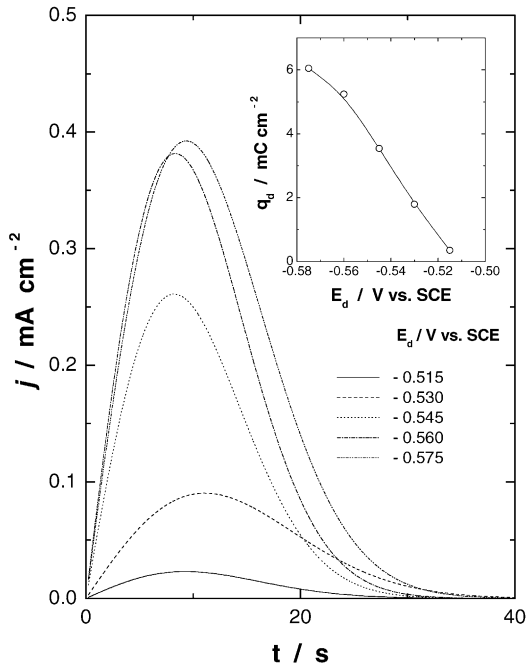

Fig. 4. Evolution of $(IN\text{-}2D)_{tc}$ current contributions at different electrodeposition potential (E_d). The inset shows the charge associate to each potential step.

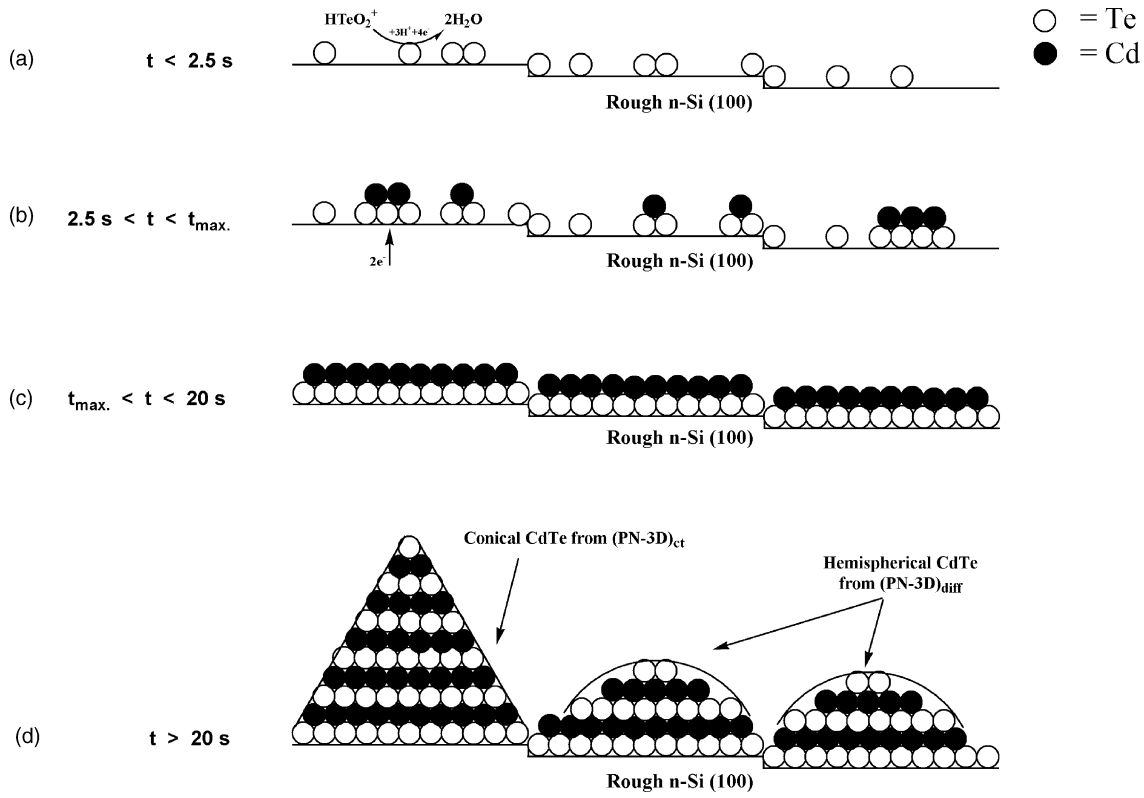

Scheme 1.

contributions involved in the overall nucleation and growth process hindering thus the 2D contribution. Moreover, the details of the evolution of the bi-dimensional current contributions at different potential steps are depicted in Fig. 4. As can be seen in the inset, the charge associated to this process tends towards a value close to 6–7 mC cm^{-2}. Considering a roughness factor of 1.0266 (see Table 1), and taking into account that the charges involved in the growth of Te and Cd monolayers are 1.0 and 0.5 mC cm^{-2} respectively, it can be appreciated that for potential values more cathodic than −0.540 V, the situation of one Cd monolayer grown onto a previously one of deposited Te is reached. This constitutes what we will label the first bi-layer. After that, the decrease of the precursor concentration in the interface (gradient concentration), and the increase of the charge transfer resistance due to the BL formation, leads to a new situation in the interface, which is very different from what has just been described.

At times greater than 20 s prevail the contributions corresponding to the progressive nucleation three dimensional charge transfer controlled growth of conical nucleus (PN-3D)$_{ct}$, (see Fig. 3b). These are originated from the reaction between the cadmium ions with the tellurium islands previously deposited to form CdTe. On the other hand, the progressive nucleation three dimensional diffusion controlled growth (PN-3D)$_{diff}$ generates hemispherical nucleus. This diffusion process found in this time interval would be related to the existence of a tellurium concentration gradient at the surface, produced by the depletion of this electroactive species at the rough silicon surface, contributing to the formation of 3D nucleus and to a rough morphology. This is probably the reason for the decrease of the diffusion coefficient obtained from the fitting in this time interval (D_{Te} = 3.5 × 10^{-7} cm^2 s^{-1}). The ex situ AFM images of the electrode surface seem to support the preceding interpretation of CdTe growth on the rough face of the n-Si wafer (see Fig. 2b). As it is seen, most of the nucleus are small and present cauliflower type morphology, but some of them form overhanging isolated conic nucleus, both accounting for the observed current/time contributions. The observed phenomenology can be summarized in Scheme 1 which accounts for the overall CdTe nucleation and growth process on rough n-type silicon surface.

4. Conclusions

The *j*/t transient responses for the formation of a CdTe film show remarkable differences in the nucleation and growth mechanism for both sides of a n-Si(1 0 0) wafer. On the flat side the current only presents an exponential decay with time but on the rough side a well developed process associated to the nucleation of a phase at the electrode surface is observed. The increase in the nucleation kinetics of the rough face is attributed to the presence of terraces that supply a significant number of edges that energetically favors the adsorption and further reduction of the redox species that are present at the interface.

The analysis of the potentiostatic j/t transients suggests that the main phenomena involved in the initial stages of the nucleation and growth of the CdTe onto the rough face of a n-Si(1 0 0) wafer is the formation of a Te–Cd bi-layer. For potentials more negatives than −0.540 V, this BL formation can be considered independent of the potential. At times greater than 20 s, the CdTe nucleation-growth process is controlled by $(PN\text{-}3D)_{ct}$ and $(PN\text{-}3D)_{diff}$ mechanisms, both accounting for the formation of conical and hemispherical nuclei, respectively. Despite of the formation of these type of 3D nuclei, they can be considered as the sum of several 2D BL discs. Ex situ AFM images of the covered surface seem to support these assumptions.

Acknowledgements

This work has been supported by a FONDECYT project (No. 8000022). E.A.D. thanks CSIC (Comisión Sectorial de Investigación Científica), Universidad de la República, Uruguay; PEDECIBA-Física, Uruguay.

References

[1] J.I. Pankove, Optical Processes in Semiconductors, Dover Publications, Inc., New York, 1975.
[2] K. Saminadayar, T. Baron, Solar cells made from widega II–Vs, in: R.N. Bhargava (Ed.), Properties of Wide Bandga II–VI Semiconductors, EMIS Datareviews Series No. 17, INSPEC, London, 1997, p. 218.
[3] Y. Xin, N.D. Browning, S. Rujirawat, S. Sivananthan, Y.P. Chen, P.D. Nellist, S.J. Pennycook, J. Appl. Phys. 84 (1998) 4292.
[4] O.K. Wu, T.J. de Lyon, R.D. Rajavel, J.E. Jensen, in: P. Capper (Ed.), Narrow Ga II–VI Compounds for Optoelectronic and Electromagnetic Applications, Chapman and Hall, London, UK, 1997, p. 97 (Chapter 4).
[5] Y. Xin, S. Rujirawat, N.D. Browning, R. Sporken, S. Sivananthan, S.J. Pennycook, N.K. Dhar, Appl. Phys. Lett. 75 (1999) 349.
[6] N.V. Sochinskii, V. Muñoz, J.M. Perez, J. Cárabe, A. Morales, Appl. Phys. Lett. 72 (1998) 2023.
[7] M.S. Han, T.W. Kang, J.H. Leem, M.H. Lee, K.J. Kim, T.W. Kim, J. Appl. Phys. 82 (1997) 6012.
[8] S. Rujirawat, Y. Xin, N.D. Browning, S. Sivananthan, D.J. Smith, S.-C.Y. Tsen, Y.P. Chen, V. Nathan, Appl. Phys. Lett. 74 (1999) 2346.
[9] H. Ebe, T. Okamoto, H. Nishino, T. Saito, Y. Nishijima, M. Uchikoshi, M. Nagashima, H. Wada, J. Electron. Mater. 25 (1996) 1358.
[10] R. Chou, M. Lin, K. Chou, Appl. Phys. Lett. 48 (1986) 523.
[11] I. Bhat, W.S. Wang, Appl. Phys. Lett. 64 (1994) 566.
[12] J.-H. Pei, C.M. Lin, D.-S. Chuu, Chin. J. Phys. 36 (1998) 44.
[13] H. Nishino, Y. Nishijima, J. Cryst. Growth 167 (1996) 488.
[14] R. Korenstein, P. Madison, P. Hallock, J. Vac. Sci. Technol. B 10 (1992) 1370.
[15] H. Tatsuoka, H. Kuwabara, Y. Nakanishi, H. Fujiyasu, J. Cryst. Growth 129 (1993) 686.
[16] Y. Sugimoto, L.M. Peter, J. Electroanal. Chem. 381 (1995) 251.
[17] Y. Sugimoto, L.M. Peter, J. Electroanal. Chem. 386 (1995) 183.
[18] J.M. Fisher, L.E.A. Berlouis, L.J.M. Sawers, S.M. MacDonald, S. Affrosman, D.J. Diskett, M.G. Astles, J. Cryst. Growth 138 (1994) 86.
[19] F. Jackson, L.E.A. Berlouis, P. Rocabois, J. Cryst. Growth 159 (1996) 200.
[20] M. Takahashi, M. Todorobaru, K. Wakita, K. Uosaki, Appl. Phys. Lett. 80 (2002) 2117.
[21] V. Pretovich, M. Haurylau, S. Volchek, Sens. Actuators A: Phys. 99 (2002) 45.
[22] R. Henríquez, R. Schrebler, H. Gómez, G. Riveros, D. Leinen, J.R. Ramos-Barrado, E.A. Dalchiele, J. Electroanal. Chem., in press.
[23] J.A. Haber, N.S. Lewis, J. Phys. Chem. B 106 (2002) 3639.
[24] A.B. Sieval, R. Linke, H. Zuilhof, E.J.R. Sudhölter, Adv. Mater. 12 (2000) 1457.
[25] L. Montès, F. Muller, F. Gaspard, R. Hérino, Thin Solid Films 297 (1997) 35.
[26] F.A. Kröger, J. Electrochem. Soc.: Solid-State Technol. 125 (1978) 2028.
[27] E. Mori, C.K. Baker, J.R. Reynolds, K. Rajeshwar, J. Electroanal. Chem. 252 (1988) 441.
[28] Y. Ein-Eli, D. Starosvetsky, Electrochem. Solid State Lett. 6 (2003) C47.
[29] E. Mori, K. Rajeshwar, J. Electroanal. Chem. 258 (1989) 415.
[30] Instrumental Methods in Electrochemistry, Horwood Publishing Limited, England, 1985, p. 383 (Chapter 9).
[31] R.K. Pandey, S.N. Sahu, S. Chandra, Handbook of Semiconductor Electrodeposition, Marcel Dekker Inc., New York, 1996, p. 61 (Chapter 3).